Hybrid-Degree Weighted T-splines and Their Application in Isogeometric Analysis

Lei Liu[a], Hugo Casquero[b], Hector Gomez[b], Yongjie Jessica Zhang[a,*]

[a] *Department of Mechanical Engineering, Carnegie Mellon University, Pittsburgh, PA 15213, USA*

[b] *Departamento de Métodos Matemáticos, Universidade da Coruña, Campus de A Coruña, 15071, A Coruña, Spain*

Abstract

In this paper, we introduce hybrid-degree weighted T-splines by means of local p-refinement and apply them to isogeometric analysis. Standard T-splines enable local h-refinement, however, they do not support local p-refinement. To increase the flexibility of T-splines so that local p-refinement is also available, we first define weighted B-spline curves of hybrid degree. Then we extend the idea to weighted T-spline surfaces of hybrid degree. A transition region is defined so as to stitch the locally p-refined region with the rest of the mesh. The transition region has the same basis function degree as the p-refined region, and the same surface continuity as the rest of the mesh. Finally, we compare the performance of odd-, even-, and hybrid-degree T-splines over an L-shaped domain governed by the Laplace equation and create high-genus surfaces using hybrid-degree weighted T-splines.

Keywords: Arbitrary Degree, Analysis-suitable T-splines, Weighted T-splines, Hybrid Degree, Local p-refinement, Isogeometric Analysis

[*] Corresponding author: Yongjie Jessica Zhang, Tel: (412) 268-5332; Fax: (412) 268-3348; Email: *jessicaz@andrew.cmu.edu*.

1. Introduction

Isogeometric analysis (IGA) adopts the same basis functions for geometric modeling and numerical analysis in order to fill the gap between these two fields [1]. Currently, the two popular basis functions in IGA are non-uniform rational B-splines (NURBS) [2–4] and T-splines [5–7]. The higher interelement continuity of these spline spaces leads to significant advantages in analysis in comparison with $\mathcal{C}^0$-continuous Lagrange polynomials used in the conventional finite element method such as, e.g., enhanced robustness in structural mechanics [8], improved accuracy per degree-of-freedom in fluid mechanics [9], among others. Fluid-structure interaction (FSI) methods benefit from the aforementioned advantages and have been an active field in IGA, both body-fitted methods [10–15] and immersed methods [16–20] have been investigated. Furthermore, the higher continuity of splines enables to solve higher-order partial differential equations in primal form [21–27] and to collocate partial differential equations in strong form [7, 28–32].

The efficiency of any computational method depends strongly on its local refinement capabilities. Unfortunately, NURBS only allow global refinement, which is an important limitation in both design and analysis. T-splines were presented as a generalization of NURBS that allow local h-refinement by introducing T-junctions. T-splines were presented in CAD in [5] and brought to analysis in [6]. An important subset of T-splines was later defined, the so-called analysis-suitable T-splines (ASTS). ASTS were mathematically shown to satisfy all the important mathematical properties of NURBS while maintaining the local h-refinement capability of T-splines. This was first demonstrated for cubic ASTS [33–36] and then for arbitrary degrees [37, 38]. The subset of ASTS is defined based on a simple topological constraint, namely, T-junction extensions from different parametric directions cannot meet with each other. T-splines with arbitrary topology can be obtained by introducing extraordinary nodes. The topological constraints in order to get cubic ASTS in the presence of extraordinary nodes were explained in [39]. Finally, these topological constraints can be relaxed by the use of weighted T-splines leading to higher flexibility [40, 41].

Local h-refinement of T-splines was first studied in [42], introducing the refinement matrix. An optimized T-junction extension algorithm was developed for local h-refinement of analysis-suitable T-splines [43]. Some adaptive h-refinement schemes have a linear computational complexity [44, 45], preserving linear independence of the basis functions. Hierarchical T-splines were proposed in [46], together with its analysis-suitability and refinability. Truncated hierarchical basis functions were also used to perform local h-refinement while ensuring partition of unity and linear independence, such as truncated hierarchical B-splines (THB) [47] and truncated hierarchical Catmull-Clark surfaces (THCCs) [48, 49].

As local h-refinement of T-splines was well studied, local p-refinement of T-splines has not been studied yet. Basis functions with elevated degree need to be defined over the whole geometry for global p-refinement. Degree elevation of B-spline curves was first studied in [50], which presents an algorithm to elevate the degree by one. Efficient algorithms were developed to raise the degree of B-spline curves/surfaces by representing a curve/surface of degree m with the linear combination of curves/surfaces of degree $m + 1$

[51, 52]. Then a fast algorithm was developed to elevate the degree by arbitrary times [53]. A software-engineering approach was presented for degree elevation of B-spline curves with competitive performance in speed and accuracy [54]. Bézier basis functions were also used for the degree elevation of B-splines, which first raise the degree of Bézier elements and then remove unnecessary knots for desired surface continuity [2]. Multi-degree splines were first introduced comprising segments with different degrees of at most 3 in one spline curve [55], where the basis functions are defined based on knot intervals like regular B-splines. Then the basis was extended with arbitrary various degrees and improved curve continuity [56]. A de Boor-like evaluation approach for multi-degree spline curves was then developed which supports local h-refinement by knot insertion and Bézier representation [57]. However, spline surfaces of multiple degree have not been studied yet.

In this work, we study weighted T-spline basis functions of both odd and even degree in detail. With a designed T-mesh splitting scheme, hybrid-degree weighted T-splines are proposed, supporting both local p-refinement and local h-refinement. The local p-refinement introduces a limited number of new control points to the T-mesh. Basis functions of different degrees are defined over the domain. The degree of basis functions of the refined region and transition region is elevated by one after local p-refinement. An L-shaped domain is parameterized with odd-, even- and hybrid-degree weighted T-splines. The Laplace equation is solved over this domain, showing the advantage of hybrid-degree T-splines. High-genus surfaces with extraordinary nodes are also parameterized with hybrid-degree weighted T-splines.

The layout of this paper is as follows. T-splines of arbitrary degree are reviewed in Section 2, together with arbitrary-degree weighted T-splines. How to generate hybrid-degree weighted T-splines is given in Section 3. Isogeometric analysis is performed over over hybrid-degree weighted T-splines in Section 4 and various high-genus surfaces are constructed. The conclusions are given in Section 5 with proposed future work.

2. Arbitrary Degree T-splines

T-splines of arbitrary degree are briefly reviewed here. For further details, we suggest the readers refer to [5–7, 42]. T-splines discussed here have the same degree in the two parametric directions. We classify them into even- and odd-degree T-splines. T-splines with $p = 2$ and $p = 3$ are used as examples to explain the definitions and show the comparison. T-splines of higher degree can be deduced analogously.

2.1. T-spline Basics

A *T-mesh* contains all the topological information of a T-spline and is composed of vertices, edges and faces. *Knot intervals* are non-negative real numbers assigned to T-mesh edges. A valid T-mesh configuration requires that the sum of knot intervals assigned to opposite edges of a face stays the same. To maintain the open knot vector property, T-meshes have $\lfloor p/2 \rfloor$ rings of edges with zero-length knot intervals, where the $\lfloor \cdot \rfloor$ represents the integer part of a real number. For example, Fig. 1(a) shows a T-mesh with one ring of edges with zero-length knot intervals. The unshaded faces have edges with zero-length intervals. This T-mesh can be used to define basis functions of either $p = 2$ or $p = 3$.

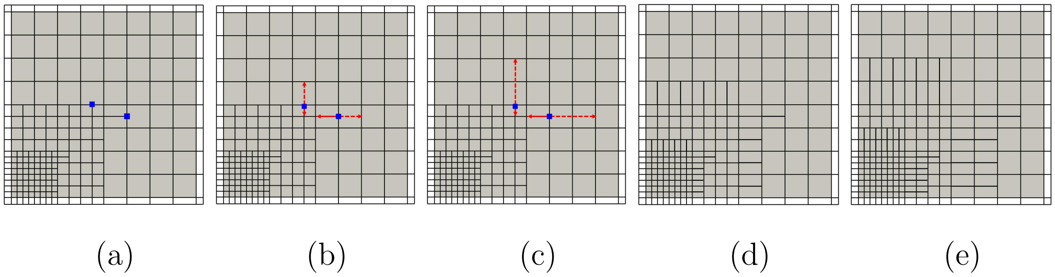

Figure 1: (a) T-mesh with two selected T-junctions marked with blue squares. The T-meshes with extensions of these two T-junctions are given in (b) when $p = 2$ and (c) when $p = 3$. The solid red lines represent edge extensions, and the dashed red lines represent face extensions. (d) and (e) show the elemental T-mesh when $p = 2$ and $p = 3$, respectively.

T-junctions are the interior vertices of valance-3 and analogous to hanging nodes in finite element meshes. The blue squares in Fig. 1(a) are two selected T-junctions. T-junction *extension* was first discussed in [36], including face extension and edge extension. A *face extension* is a line obtained by moving from the T-junction along the missing edge direction until $\lfloor (p+1)/2 \rfloor$ orthogonal edges are encountered. An *edge extension* is a line obtained by moving opposite to the face extension direction until $\lfloor p/2 \rfloor$ orthogonal edges are encountered. For example in Fig. 1(b, c), the face extensions are marked with dashed red lines, and edge extensions are marked with solid red lines when $p = 2$ and $p = 3$. For general analysis-suitable T-splines of arbitrary degree, it is required that T-junction extensions cannot meet with each other from different parametric directions [37]. Edge and face extensions are used to check if analysis-suitable requirements are satisfied by the T-mesh. By only drawing all the face extensions and excluding faces with zero-length interval edges in the T-mesh, we obtain the elemental T-meshes as shown in Fig. 1(d, e).

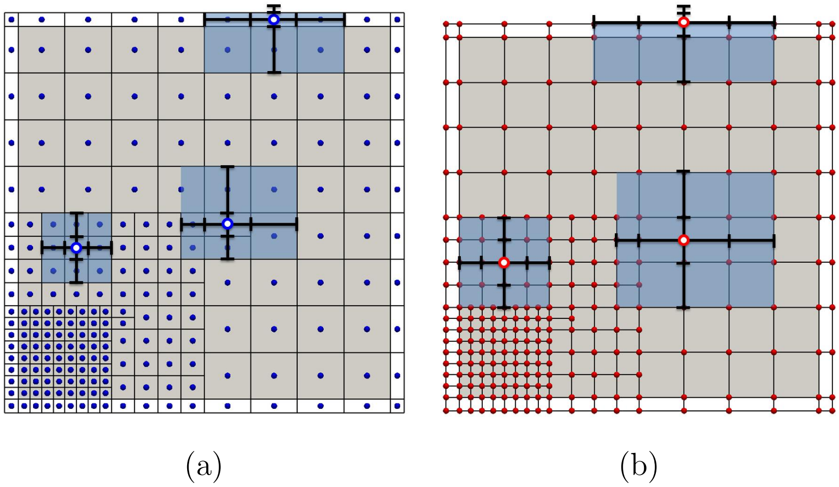

Figure 2: Three basis functions of different degrees are given with their local knot vectors and supported regions shaded with light blue. (a) $p = 2$ with blue dots representing the anchors; and (b) $p = 3$ with red dots representing the anchors.

Anchors are used to determine the local knot vectors and each anchor is associated with one T-spline basis function. For even degree T-splines, anchors are placed at the centers of the faces. As shown in Fig. 2(a), each blue dot represents an anchor. For odd degree T-splines, anchors are placed at each vertex, represented with red dots in Fig. 2(b). Local *knot interval vectors* are inferred from the T-mesh. A local knot interval vector in the ξ direction is a sequence of knot intervals $\Delta\widehat{\Xi} = \{\Delta\widehat{\xi}_1, \Delta\widehat{\xi}_2, \cdots, \Delta\widehat{\xi}_{p+1}\}$. There are $p+1$ interval values in each local knot interval vector. The corresponding local knot vector is a non-decreasing knot sequence $\widehat{\Xi} = \{\widehat{\xi}_1, \widehat{\xi}_2, \cdots, \widehat{\xi}_{p+2}\}$ such that $\Delta\widehat{\xi}_i = \widehat{\xi}_{i+1} - \widehat{\xi}_i$. Each anchor is assigned with two local knot vectors along two parametric directions.

To obtain local knot interval vectors, we shoot rays in each parametric direction (both positive and negative) to place a segment centered in the anchor crossing exactly $p + 2$ orthogonal edges. Note that "centered in the anchor" means that the segment crosses the same number of orthogonal edges on the left- and right-hand sides of the anchor, and spans a particular set of $p + 1$ edges. The knot interval values of the spanned edges are placed into the local knot interval vector consecutively. Zero-length edges are appended when a boundary is crossed before enough orthogonal edges are found.

Based on the local knot interval vectors, local knot vectors are obtained and T-spline basis functions are defined. If a T-spline basis function has non-zero value over one region covered in the T-mesh, then it has support over the geometry in the physical domain extracted from that region. The light blue regions in Fig. 2 show the support of different T-spline basis functions associated with the selected anchors.

T-splines of arbitrary degree are defined element-wise. For element e in the elemental T-mesh, suppose $\mathbf{N}^e = \{N_i^e(\xi, \eta)\}_{i=1}^{n^e}$ is the vector of T-spline basis functions having support over e. $N_i^e(\xi, \eta)$ is the basis function mapped to the parent element $\square = [-1, 1]^2$ with the affine map introduced in [58]. Then the T-spline geometry is defined by the element geometric map, $\mathbf{x}^e : \square \to \Omega^e$, from the parent element domain to the physical domain as

$$\mathbf{x}^e = \frac{\sum_{i=1}^{n^e} w_i \mathbf{P}_i^e N_i^e(\xi, \eta)}{\sum_{i=1}^{n^e} w_i N_i^e(\xi, \eta)}, \tag{1}$$

where $\mathbf{P}_i^e$ is the corresponding control point of the basis function $N_i^e(\xi, \eta)$, and w_i^e is the corresponding weight. Note that $\mathbf{P}_i^e$, w_i^e are all mapped from global to local numbering by the IEN array [58] such that $\mathbf{P}_i^e = \mathbf{P}_{\mathrm{IEN}(i,e)}$ and $w_i^e = w_{\mathrm{IEN}(i,e)}$. The element control points $\mathbf{P}^e$ is a matrix of dimension $n^e \times d_s$, where d_s is the spatial dimension. Analysis-suitable T-splines of arbitrary degree satisfy polynomial partition of unity, which means $\sum_{i=1}^{n^e} N_i^e(\xi,\eta) = 1$. When $w_i^e = 1.0$ for any $\mathbf{P}_i^e$, Eqn. (1) is simplified as

$$\mathbf{x}^e = \sum_{i=1}^{n^e} \mathbf{P}_i^e N_i^e(\xi,\eta). \tag{2}$$

In the following, we set the weights of all the control points are 1.0 for the sake of brevity.

2.2. Bézier Element Extraction

Based on the Bézier extraction algorithm [58, 59], T-spline basis functions can be represented as linear combinations of Bézier basis functions. Each element in the elemental T-mesh corresponds to one Bézier element. The e^{th} Bézier element in the physical domain can be represented as

$$\mathbf{x}^e = \sum_{i=1}^{n^e} \mathbf{P}_i^e N_i^e(\xi,\eta) = \sum_{i=1}^{n^e} \mathbf{P}_i^e \sum_{j=1}^{(p+1)^2} M_{ij}^e B_j(\xi,\eta), \tag{3}$$

where $B_j(\xi,\eta)$ is the j^{th} Bézier basis function defined on the parent element, and M_{ij}^e is the Bézier extraction coefficient. By converting Eqn. (3) to matrix format, we have

$$\mathbf{x}^e = (\mathbf{P}^e)^T \mathbf{N}^e = (\mathbf{P}^e)^T \mathbf{M}^e \mathbf{B}, \tag{4}$$

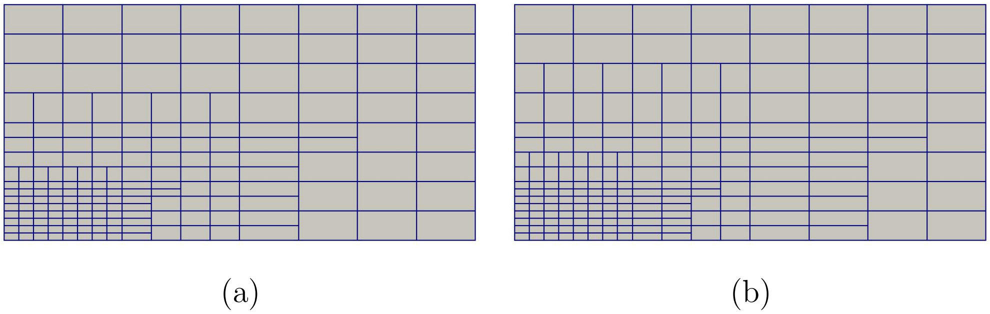
(a) (b)

Figure 3: Locally h-refined T-splines with Bézier representation. (a) $p = 2$; and (b) $p = 3$.

where $\mathbf{P}^e$ is the matrix of control points, $\mathbf{M}^e$ is the Bézier extraction matrix, and $\mathbf{B}$ is the vector of Bézier basis functions. Eqn. (4) is the Bézier element representation of T-splines. Fig. 3 shows a rectangular domain parameterized with locally h-refined T-splines and Bézier element representations when $p = 2$ and $p = 3$.

2.3. Arbitrary-Degree Weighted T-splines

The subset of ASTS is defined based on a simple topological constraint, namely, horizontal T-junction extensions cannot meet with vertical T-junction extensions. If the quadtree subdivision algorithm is applied to a T-mesh, the resulting T-mesh may violate the topological constraint mentioned above and polynomial partition of unity may not be satisfied. However, polynomial partition of unity can be recovered through the use of weighted T-splines [40].

Weighted T-splines enable to use more simple and localized h-refinement strategies over the T-mesh such as, e.g., quadtree subdivision. For a T-spline basis function $N_j(\xi, \eta)$ with corresponding control point $\mathbf{P}_j$ obtained from the knot insertion algorithm, if partition of unity is satisfied in all the support of $N_j(\xi, \eta)$, then the weighted T-spline basis function $\widehat{N}_j(\xi, \eta)$ equals to $N_j(\xi, \eta)$ and $\widehat{\mathbf{P}}_j$ equals to $\mathbf{P}_j$. Otherwise for $N_j(\xi, \eta)$, the weighting coefficients of children basis functions [40] or extracted Bézier basis functions [41] are modified to obtain $\widehat{N}_j(\xi, \eta)$. The control points associated with modified basis functions are computed solving a linear system [40]. The detailed weighting coefficient modification algorithm is explained as follows.

Given a T-mesh, the weighted T-spline of degree p on the e^{th} Bézier element is defined as

$$\mathbf{x}^e = \sum_{j=1}^{n^e} \widehat{\mathbf{P}}_j^e \widehat{N}_j^e(\xi,\eta) = \sum_{j=1}^{n^e} \widehat{\mathbf{P}}_j^e \sum_{k=1}^{(p+1)^2} \widehat{M}_{jk}^e B_k(\xi,\eta) = (\widehat{\mathbf{P}}^e)^T \widehat{\mathbf{M}}^e \mathbf{B}, \tag{5}$$

where $\widehat{N}^e(\xi,\eta)$ are the weighted T-spline basis functions with support over this Bézier element, $\widehat{\mathbf{P}}_j^e$ are the corresponding control points. $\widehat{\mathbf{M}}^e$ is the matrix which transfers weighted T-spline basis functions to Bézier basis functions. $B_k(\xi,\eta)$ is the Bézier basis function. The IEN array is also used here to handle the mapping from global to local numbering.

To obtain $\widehat{\mathbf{M}}^e$, we first calculate the Bézier transformation matrix $\mathbf{M}^e$ for regular T-spline basis functions $N_j^e(\xi,\eta)$. Note that with $\mathbf{M}^e$, partition of unity may not be satisfied everywhere. For a Bézier basis function $B_k(\xi,\eta)$, the summation of calculated weighting coefficients $(\sum_{j=1}^{n^e} M_{jk}^e)$ from $N_j^e(\xi,\eta)$ may not be 1.0. We modify $\mathbf{M}^e$ to $\widehat{\mathbf{M}}^e$ such that

$$\widehat{M}_{jk}^e = \frac{M_{jk}^e}{\sum_{i=1}^{n^e} M_{ik}^e}. \tag{6}$$

Consequently, the regular T-spline basis functions are replaced with weighted T-spline basis functions and

$$\sum_{j=1}^{n^e} \widehat{M}_{jk}^e = 1, \;\; k = 1, 2, \cdots, (p+1)^2 \tag{7}$$

is always satisfied. Since Bézier basis functions satisfy partition of unity, we have

$$\sum_{j=1}^{n^e} \widehat{N}_j^e(\xi,\eta) = \sum_{j=1}^{n^e} \sum_{k=1}^{(p+1)^2} \widehat{M}_{jk}^e B_k(\xi,\eta) = 1, \tag{8}$$

and weighted T-splines always satisfy polynomial partition of unity.

Note that we are normalizing each column of $\mathbf{M}^e$ to obtain $\widehat{\mathbf{M}}^e$ according to Eqn. (6). This modification only involves elementary matrix operation and does not change the rank of the matrix. Since $\mathbf{M}^e$ is in full-rank, $\widehat{\mathbf{M}}^e$ is also in full-rank. So the weighted T-splines of arbitrary degree are linearly independent [36, 40, 41].

3. Hybrid-Degree Weighted T-splines

In this section, we introduce our algorithm to construct hybrid-degree weighted T-splines by means of local p-refinement. We first introduce hybrid-degree B-spline curves, and then generalize the ideas to hybrid-degree weighted T-spline surfaces.

3.1. Hybrid-Degree B-spline Curves

Generally for B-splines, global degree elevation increases the degree of all the basis functions. Suppose a cubic B-spline is defined on the open knot vector $U = \{u_0, u_0, u_0, u_0, u_1, u_2, ..., u_n, u_n, u_n, u_n\}$. There are n+3 basis functions. To elevate it to quartic, each unique knot value in U is duplicated once to form the new open knot vector $\overline{U} = \{u_0, u_0, u_0, u_0, u_0, u_1, u_1, u_2, u_2, ..., u_n, u_n, u_n, u_n, u_n\}$, based on which $2n + 3$ new quartic B-spline basis functions are defined. The detailed algorithm can be found in [2]. B-spline global degree elevation can increase the degree of basis functions without modifying the geometry [2]. The disadvantages are that a lot of new control points are calculated and the interelement continuity is not increased.

To construct hybrid-degree B-spline curves by means of local p-refinement, we define the spline basis functions on local knot vectors instead of using a global knot vector, which is analogous to what is done in T-splines. Fig. 4(a) shows part of a cubic B-spline curve in the index space, where the orange edge has knot interval value 0 and the black edges have knot interval value 1.

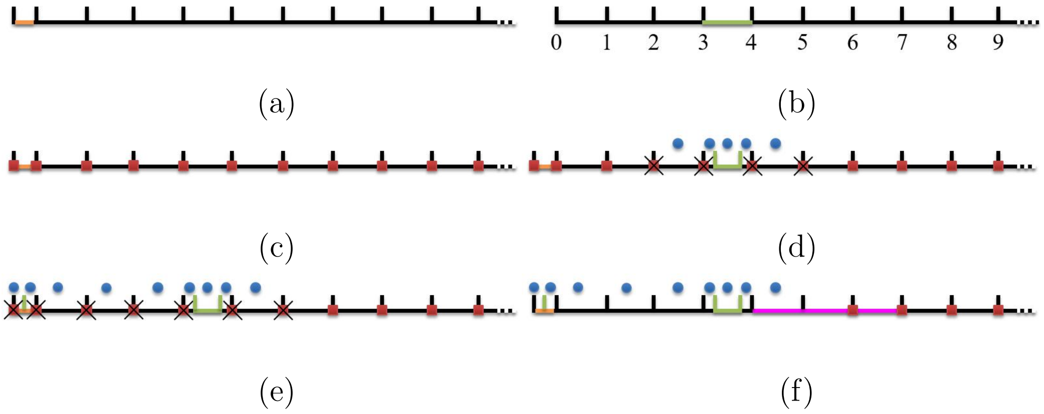

Figure 4: Local p-refinement of B-splines of $p = 3$. (a) The mesh of B-spline in the index space, where the orange edge has knot interval value 0, and the black edges have knot interval value 1; (b) the mesh in the parametric space, where the green edge is set as the hybrid boundary; (c) the red squares represent the anchors to define cubic basis functions; (d) for the green edge, the corresponding anchors to define supporting cubic and quartic basis functions of are represented with the crossed-out red squares and blue circles, respectively; (e) quartic basis functions are defined on the p-refined region; and (f) the resulting anchors to define cubic and quartic basis functions . Both cubic and quartic basis functions have support over the magenta transition region.

The B-spline in the parametric space is given in Fig. 4(b) with parametric values. The red squares in Fig. 4(c) represent the anchors to define cubic basis functions before p-refinement. To perform local p-refinement, we define basis functions of degree $p + 1$ only on the refined region.

Knot Insertion. A *Hybrid boundary* is the edge where we add knots to its ends so as to stitch the p-refined region with the rest of the curve. In Fig. 4(b), suppose we want to perform local p-refinement to the region $u \leq 4$, then the edge marked in green is the hybrid boundary.

There are four cubic basis functions ($N_i^3(u), 4 \leq i \leq 7$) that have support over the green edge before p-refinement. They are defined on local knot vectors $\{0, 1, 2, 3, 4\}$, $\{1, 2, 3, 4, 5\}$, $\{2, 3, 4, 5, 6\}$, $\{3, 4, 5, 6, 7\}$, respectively. The corresponding anchors are represented with crossed-out red squares in Fig. 4(d). To perform local p-refinement, two new knots (3 and 4) are inserted. There are five quartic basis functions ($N_i^4(u), 5 \leq i \leq 9$) with support over the green edge (see Fig. 5(b)). They are defined on local knot vectors $\{0, 1, 2, 3, 3, 4\}$, $\{1, 2, 3, 3, 4, 4\}$, $\{2, 3, 3, 4, 4, 5\}$, $\{3, 3, 4, 4, 5, 6\}$, $\{3, 4, 4, 5, 6, 7\}$, respectively, and the corresponding anchors are represented with blue circles in Fig. 4(d). To preserve the open knot vector property, zero knot is also inserted, shown in Fig. 4(e, f).

Definition of Basis Functions. We disactivate the basis functions of degree p having support over the p-refined region and activate basis functions of degree *p+1* that have support over this region. In the *p-refined region* ($u \leq 4$), quartic basis functions are defined. The final anchors to define basis functions over the whole domain are shown in Fig. 4(f). The defined basis functions before and after local p-refinement as depicted in Fig. 4 are shown in Fig. 5(a, b). In Fig. 5(a), the dashed red lines are the removed cubic basis functions from the p-refined region. The solid blue lines in Fig. 5(b) show the newly defined quartic basis functions in the p-refined region.

Transition Region. A *Transition region* connects the refined region and the *unchanged region.* Only basis functions of degree $p + 1$ have support over the refined region ($0 \leq u \leq 4$ in Fig. 5(b)). Only basis functions of degree p have support over the unchanged region ($u \geq 7$ in Fig. 5(b)). Basis functions of both degree p and $p + 1$ have support over the transition region ($4 \leq u \leq 7$ in Fig. 5(b)). We use hybrid-degree B-splines to represent the

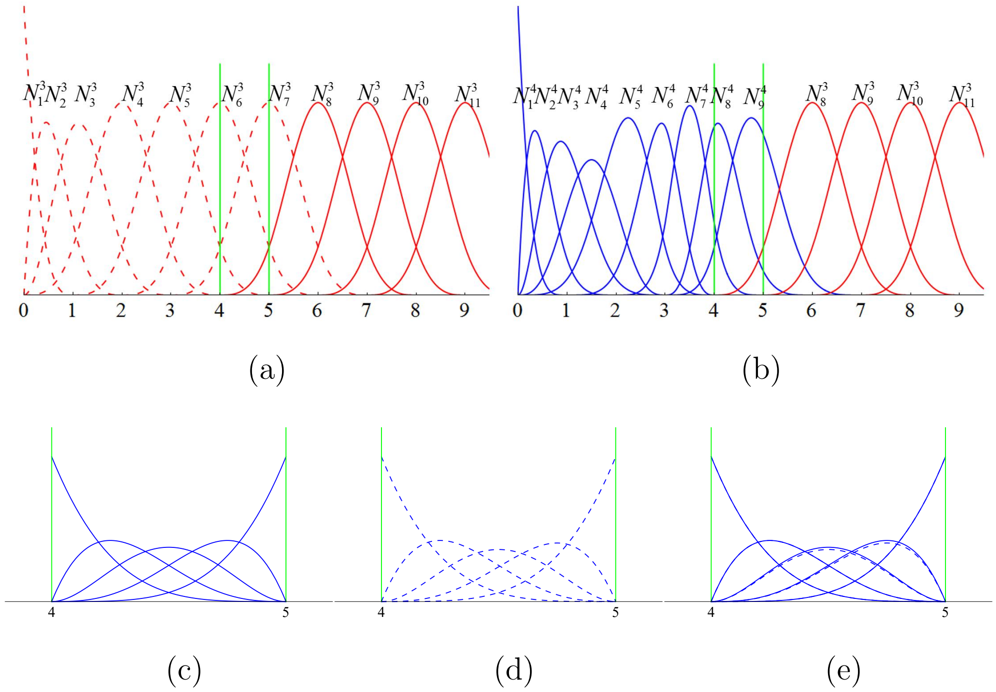

Figure 5: (a) Basis functions of $p = 3$ (red), where the dashed red basis functions are removed; (b) basis functions of $p = 4$ (blue) are defined on the refined region; (c) Bézier basis functions of $p = 4$ over region $4 \leq u \leq 5$; (d) weighted Bézier basis functions obtained from Eqn. (13); and (e) the difference between (c) and (d).

geometry over this region. Let us take the edge at $4 \leq u \leq 5$ as an example. There is one cubic basis function ($N_8^3(u)$) and three quartic basis functions ($N_i^4(u), 7 \leq i \leq 9$) having support over it, shown in Fig. 5(b). To define the geometry, we have

$$\mathbf{x} = \mathbf{P}_8^3 N_5^3(u) + \sum_{i=7}^{9} \mathbf{P}_i^4 N_i^4(u), \tag{9}$$

where $\mathbf{P}_8^3$, $\mathbf{P}_i^4$ are the corresponding control points of the basis functions $N_8^3(u)$ and $N_i^4(u)$ respectively. $\mathbf{P}_8^3$ is the 8^{th} vertex in the control polygon of the original cubic B-spline. $\mathbf{P}_i^4$ are the center points of each control polygon edge, which are obtained by linear interpolation of the two vertices of the polygon edge. By representing the B-spline basis functions with Bézier basis functions, we have

$$\begin{aligned}\mathbf{x} &= \mathbf{P}_8^{e,p} \sum_{j=1}^{4} M_{8j}^{e,p} B_j^p(u) + \sum_{i=7}^{9} \mathbf{P}_i^{e,p+1} \sum_{k=1}^{5} M_{ik}^{e,p+1} B_k^{p+1}(u) \\ &= \sum_{j=1}^{4} \mathbf{Q}_j^{e,p} B_j^p(u) + \sum_{k=1}^{5} \mathbf{Q}_k^{e,p+1} B_k^{p+1}(u),\end{aligned} \tag{10}$$

where $p = 3$, $M_{8j}^{e,p}$ and $M_{ik}^{e,p+1}$ are the Bézier extraction coefficients. $\mathbf{Q}_j^{e,p}$ and $\mathbf{Q}_k^{e,p+1}$ are the Bézier control points. Based on the degree elevation algorithm for Bézier elements [2], we have

$$\mathbf{Q}_i^{e,p+1} = (1 - \frac{i-1}{p+1})\mathbf{Q}_i^{e,p} + \frac{i-1}{p+1}\mathbf{Q}_{i-1}^{e,p}, \quad i = 1, 2, \cdots, p+2. \tag{11}$$

When $i = 1$, $\frac{i-1}{p+1} = 0$ and when $i = p+2$, $1 - \frac{i-1}{p+1} = 0$. The undefined $Q_0^{e,p}$ and $\mathbf{Q}_{p+2}^{e,p}$ do not jeopardize the integrity of Eqn. (11) and we set them as 0. We move the superscript p of control points and Bézier extraction matrix to subscript for convenience, and convert Eqn. (10) to matrix format

$$\mathbf{x}^e = (\mathbf{P}_p^e)^T \mathbf{M}_p^e \mathbf{B}^p + (\mathbf{P}_{p+1}^e)^T \mathbf{M}_{p+1}^e \mathbf{B}^{p+1} = (\mathbf{Q}_p^e)^T \mathbf{B}^p + (\mathbf{Q}_{p+1}^e)^T \mathbf{B}^{p+1}. \tag{12}$$

With Eqn. (11), Eqn. (12) is converted to

$$\begin{aligned}\mathbf{x}^e &= (\mathbf{Q}_p^e)^T \mathbf{T}_p^{p+1} \mathbf{B}^{p+1} + (\mathbf{Q}_{p+1}^e)^T \mathbf{B}^{p+1} = (\mathbf{P}_p^e)^T \mathbf{M}_p^e \mathbf{T}_p^{p+1} \mathbf{B}^{p+1} + (\mathbf{P}_{p+1}^e)^T \mathbf{M}_{p+1}^e \mathbf{B}^{p+1} \\ &= ((\mathbf{P}_p^e)^T \mathbf{M}_p^e \mathbf{T}_p^{p+1} + (\mathbf{P}_{p+1}^e)^T \mathbf{M}_{p+1}^e) \mathbf{B}^{p+1} = \mathbf{R}^T \overline{\mathbf{M}}_{p+1}^e \mathbf{B}^{p+1},\end{aligned} \tag{13}$$

where $\mathbf{T}_p^{p+1}$ is obtained from Eqn. (11), $\mathbf{R}$ are the control points. $\overline{\mathbf{M}}_{p+1}^e$ is the transformation matrix, and $\mathbf{B}^{p+1}$ represent Bézier basis functions.

Partition of unity is not satisfied here. We recover partition of unity through the use of weighted T-splines as explained in Section 2.3. Fig. 5(c) shows the five quartic Bézier basis functions. The calculated weights of the five Bézier basis functions obtained from $\overline{\mathbf{M}}_{p+1}^{e}$ are $1.0, 1.0, 0.95833, 0.95833$ and 1.0, respectively. The weighted Bézier basis functions are shown in Fig. 5(d). The differences are shown in Fig. 5(e). Finally Eqn. (13) is converted to

$$\mathbf{x}^e = \mathbf{R}^T \widehat{\mathbf{M}}_{p+1}^{e} \mathbf{B}^{p+1}, \tag{14}$$

which is used to define the hybrid-degree weighted B-splines over the transition region.

Remark 3.1. The hybrid B-spline defined over the transition region is of degree $p + 1$, since we performed degree elevation to the Bézier basis functions of degree p. But the surface continuity is C^{p-1}, which is the same as the unchanged region. The reason is that basis functions of degree p have support over this region.

3.2. Local p-refinement of T-splines

To explain local p-refinement of T-splines, we define the graph connecting all the faces to introduce new zero-length edges as the hybrid boundary. There are two types of hybrid boundaries, namely the *interior boundary* and the *extended boundary.* Interior boundaries are the loops within the domain. Extended boundaries contain faces lying on the boundary of the geometry. We constrain that the hybrid boundaries cannot be reached by face extension of any T-junction. In this way, T-junctions do not influence the faces lying on the hybrid boundaries.

There are mainly three steps to perform local p-refinement. We first determine the local parametric directions to split the faces on the hybrid boundaries. Then we split the faces along the detected directions to introduce zero-length interval edges to the T-mesh. After the splitting we define higher order basis functions over the p-refined region. The last step is to decide the active original basis functions and calculate the new control points.

Here we take the T-mesh in Fig. 6(a) as an example. Since there is only one ring of edges with zero-length intervals on the boundary of the T-mesh, both basis functions of $p = 3$ and $p = 2$ can be defined on it. The three steps are explained mainly based on odd degree T-splines. Even degree T-splines are used to explain the difference and show the comparison.

Local Splitting Direction Detection (Step 1). Fig. 6(a) and (c) show the interior and extended hybrid boundaries of the T-mesh, marked in light green and light blue, respectively. We split the faces on the hybrid boundaries to introduce zero-length interval edges across them. For a pair of neighboring faces sharing an edge on the hybrid boundary, the splitting direction is perpendicular to that edge. If a face has edges of two different directions shared by other faces on the hybrid boundary, it should be split in both directions. For example the faces on the corners of the hybrid boundaries in Fig. 6(a) and (c) should be split in both directions.

T-mesh Splitting and Basis Function Definition (Step 2). With the detected splitting directions, we split the faces on the hybrid boundaries as shown in Fig. 6(b). If one face should be split in one direction, we split it into three new faces. The new face in the middle has the same edge interval values as the original faces, see the light green faces. The other two have zero-length interval across the splitting direction, see the unshaded faces. If a face should be split in both directions, nine new faces are generated. The

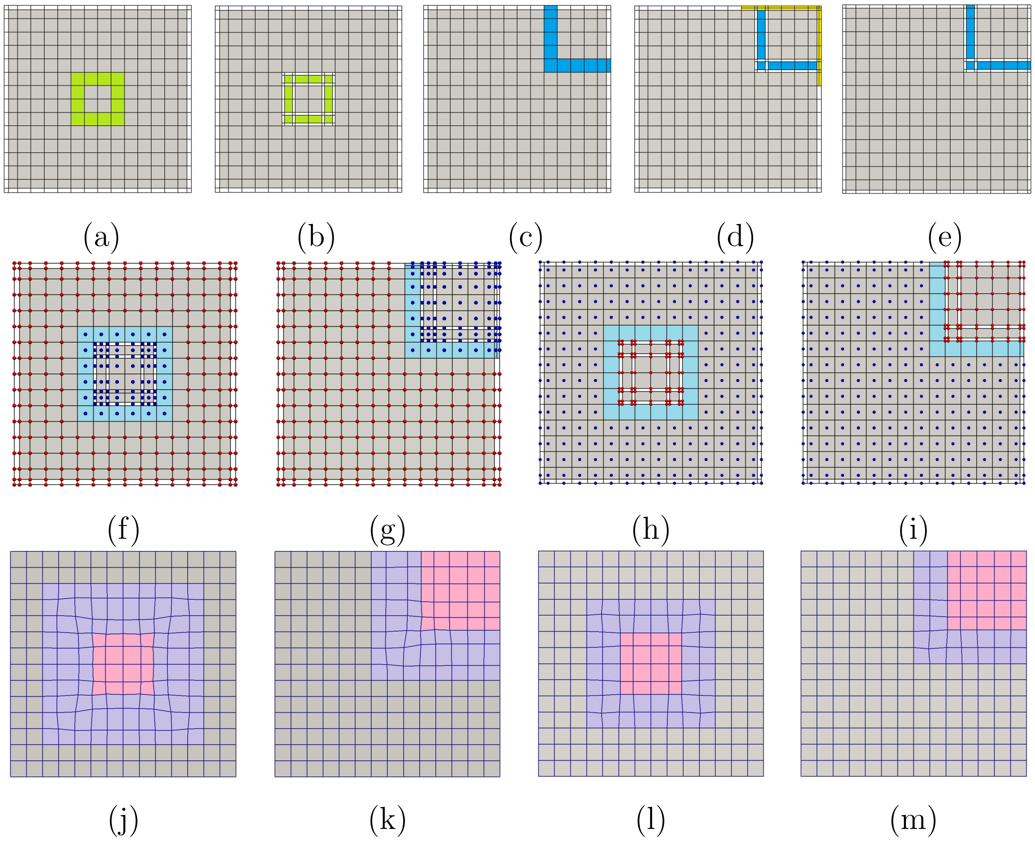

Figure 6: Local p-refinement of T-splines with $p = 3$ and $p = 2$. (a) Interior boundary marked in light green; (b) T-mesh splitting result of (a); (c) extended boundary marked in light blue; (d) T-mesh splitting result of (c) when $p = 3$; The yellow faces on the domain boundary are split to preserve the open knot vector property; (e) T-mesh splitting result of (c) when $p = 2$; (f-i) selected anchors to define active basis functions, where the adjacent region is marked in cyan, the red and blue dots represent anchors located at corners and centers of T-mesh faces, respectively, with $p = 3$ in (f, g) and $p = 2$ in (h, i); (j-m) the hybrid T-splines with Bézier representation, where the transition region is marked in purple, and the p-refined region is marked in pink, with $p = 3$ in (j, k) and $p = 2$ in (l, m).

one in the middle has the same interval values as the original one. The other ones have either two or four edges with zero-length interval.

In the p-refined region, if there are faces on the boundary of the domain, then the open knot vector property should be satisfied after T-mesh splitting. When performing local p-refinement to T-splines of odd degree, one new boundary layer with zero-length interval edges is introduced. For T-mesh in Fig. 6(c), if $p = 3$, there is one layer of faces with zero-length intervals. After refining it to $p = 4$, there should be two layers. We equally split the faces on the geometric boundary to two smaller ones. The splitting follows the direction of the geometry boundary. If the face is at the corner of the geometry, it is equally split into four smaller ones. In Fig. 6(d), those faces marked in yellow are the newly generated faces with zero-length intervals. If p is even, no boundary face splitting is required to satisfy the open knot vector property. In Fig. 6(e), faces on the geometric boundary remain unchanged, except those on the extended hybrid boundary.

After T-mesh splitting, we place anchors on both the corners and the centers of T-mesh faces. Local knot vectors are inferred for each anchor. For an anchor at the corner, a T-spline basis function of odd degree is defined. Whereas for an anchor at the center, a T-spline basis function of even degree is defined.

We define an *adjacent region* as the first-ring neighborhood of the hybrid boundary beyond the p-refined region. In Fig. 6(f - i), the adjacent regions are marked in cyan. All the basis functions of degree $p + 1$ in the p-refined region are set as active. All basis functions of degree p beyond the adjacent region are also set as active. When p is odd, the basis functions of degree $p + 1$ at the face center in the adjacent region are set as active. In Fig. 6(f, g), the anchors to define active cubic basis functions are represented with red dots. The anchors to define active p-refined quartic basis functions are represented with blue dots. When p is even, the basis functions of degree $p+1$ at the corners shared by the adjacent region and the hybrid boundary are set as active. In Fig. 6(h, i), the anchors to define active quadratic basis functions are represented with blue dots, and the anchors to define active cubic basis functions are represented with red dots.

Control Point Calculation (Step 3). Local p-refinement may slightly change the geometry. The refinement algorithms introduced in [2] to calculate control points cannot be used here because zero-length interval edges are only introduced along the hybrid boundary. Here we introduce a direct way to calculate the new control points from the original ones by linear interpolation.

We place five control points on each T-mesh element. Four are at the corners and the last one is in the center. If p is odd, we use corner points to interpolate the center control points for the new basis functions of degree $p+1$. For example in Fig. 7(a), a center control point $\mathbf{C}_1$ is calculated by

$$\mathbf{C}_1 = \frac{\mathbf{P}_1 + \mathbf{P}_2 + \mathbf{P}_3 + \mathbf{P}_4}{4}, \tag{15}$$

where $\mathbf{P}_1 \sim \mathbf{P}_4$ are four control points at the corners. If p is even, we use center points to perform the interpolation. In Fig. 7(b), a corner control point $\mathbf{P}_1$ is calculated by

$$\mathbf{P}_1 = \frac{\Delta\xi_2\Delta\eta_2\mathbf{C}_1 + \Delta\xi_1\Delta\eta_2\mathbf{C}_2 + \Delta\xi_1\Delta\eta_1\mathbf{C}_3 + \Delta\xi_2\Delta\eta_1\mathbf{C}_4}{(\Delta\xi_1 + \Delta\xi_2)(\Delta\eta_1 + \Delta\eta_2)}, \tag{16}$$

where $\mathbf{C}_1 \sim \mathbf{C}_4$ are four control points at the centers of the elements which share $\mathbf{P}_1$. After the T-mesh splitting and control point calculation, we can define the hybrid-degree weighted T-splines.

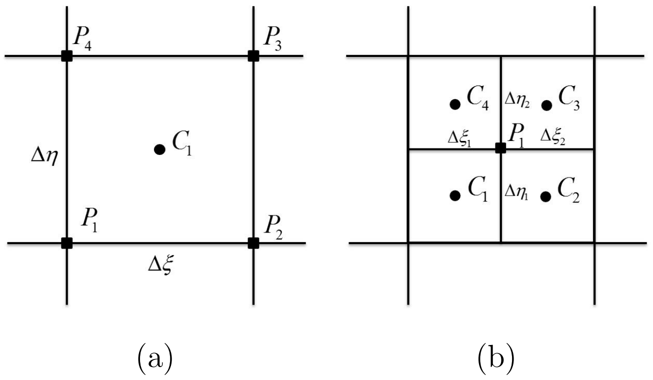

Figure 7: Interpolation scheme to obtain new control points. (a) Using corner control points to calculate the center control point; and (b) using center control points to calculate the corner control point.

3.3. Hybrid-Degree Weighted T-spline Construction

We define the hybrid-degree weighted T-splines with Bézier element representation. In the p-refined region, only basis functions of degree $p+1$ have support over extracted Bézier elements. In the unchanged region, only basis functions of degree p have support over extracted Bézier elements. Both basis functions of degree p and $p+1$ have support over the Bézier elements extracted from the transition region. There are $\lfloor (p+1)/2 \rfloor + 1$ rings of elements in the transition region (see Fig. 6(j-m)).

Bézier elements in the p-refined or unchanged region are calculated using Eqn. (4). Over the transition region, the hybrid-degree T-spline for the e^{th} element is defined as

$$\mathbf{x}^e = \sum_m \mathbf{P}^e_m N^{e,p}_m(\xi,\eta) + \sum_n \mathbf{C}^e_n N^{e,p+1}_n(\xi,\eta) \tag{17}$$

when p is odd, and

$$\mathbf{x}^e = \sum_m \mathbf{C}^e_m N^{e,p}_m(\xi,\eta) + \sum_n \mathbf{P}^e_n N^{e,p+1}_n(\xi,\eta) \tag{18}$$

when p is even. In Eqns. (17)-(18), $\mathbf{P}^e_m$, $\mathbf{P}^e_n$ are the corner control points, and $\mathbf{C}^e_n$, $\mathbf{C}^e_m$ are the center control points. $N^{e,p}_m(\xi,\eta)$ and $N^{e,p+1}_n(\xi,\eta)$ are the active T-spline basis functions defined on the T-mesh after refinement. We first derive the expression for T-splines of hybrid degrees when p is odd.

With the Bézier extraction algorithm, Eqn. (17) is converted to

$$\begin{aligned}\mathbf{x}^e &= \sum_m \mathbf{P}^e_m \sum_{j=1}^{(p+1)^2} M^{e,p}_{mj} B^p_j(\xi,\eta) + \sum_n \mathbf{C}^e_n \sum_{k=1}^{(p+2)^2} M^{e,p+1}_{nk} B^{p+1}_k(\xi,\eta) \\ &= \sum_{\alpha=1}^{p+1}\sum_{\beta=1}^{p+1} \mathbf{Q}^{e,p}_{\alpha,\beta} B^p_{\alpha,\beta}(\xi,\eta) + \sum_{\alpha=1}^{p+2}\sum_{\beta=1}^{p+2} \mathbf{Q}^{e,p+1}_{\alpha,\beta} B^{p+1}_{\alpha,\beta}(\xi,\eta),\end{aligned} \tag{19}$$

where $M^{e,p}_{mj}$ and $M^{e,p+1}_{nk}$ are the Bézier extraction coefficients. $B^p_j(\xi,\eta)$ and $B^{p+1}_k(\xi,\eta)$ are Bézier basis functions of degree p and $p+1$. We have $j = (\alpha-1)\times(p+1)+\beta$, and $k = (\alpha-1)\times(p+2)+\beta$. $\mathbf{Q}^{e,p}_{\alpha,\beta}$ and $\mathbf{Q}^{e,p+1}_{\alpha,\beta}$ are the Bézier control points.

We elevate the Bézier basis functions of degree p to $p+1$ by extending Eqn. (11) to 2D such that

$$\begin{aligned}\mathbf{Q}^{e,p+1}_{\alpha,\beta} &= (1-\frac{\alpha-1}{p+1})((1-\frac{\beta-1}{p+1})\mathbf{Q}^{e,p}_{\alpha,\beta} + \frac{\beta-1}{p+1}\mathbf{Q}^{e,p}_{\alpha,\beta-1}) \\ &+ \frac{\alpha-1}{p+1}((1-\frac{\beta-1}{p+1})\mathbf{Q}^{e,p}_{\alpha-1,\beta} + \frac{\beta-1}{p+1}\mathbf{Q}^{e,p}_{\alpha-1,\beta-1}),\end{aligned} \tag{20}$$

where $\alpha = 1,2,\cdots,p+2$, and $\beta = 1,2,\cdots,p+2$. Similarly, the undefined $Q^{e,p}_{0,\beta}$, $Q^{e,p}_{\alpha,0}$, $Q^{e,p}_{p+2,\beta}$ and $\mathbf{Q}^{e,p}_{\alpha,p+2}$ do not jeopardize the integrity of Eqn. (20) since they all have 0 coefficients, and they are set as 0. To obtain the matrix format of Eqn. (19), we move superscript p of Bézier control points and

Bézier extraction matrix to subscript for convenience. We have

$$\mathbf{x}^e = (\mathbf{P}^e)^T \mathbf{M}_p^e \mathbf{B}^p + (\mathbf{C}^e)^T \mathbf{M}_{p+1}^e \mathbf{B}^{p+1} = (\mathbf{Q}_p^e)^T \mathbf{B}^p + (\mathbf{Q}_{p+1}^e)^T \mathbf{B}^{p+1}. \tag{21}$$

With Eqn. (20), Eqn. (21) is converted to

$$\begin{aligned}\mathbf{x}^e &= (\mathbf{Q}_p^e)^T \mathbf{T}_p^{p+1} \mathbf{B}^{p+1} + (\mathbf{Q}_{p+1}^e)^T \mathbf{B}^{p+1} = (\mathbf{P}^e)^T \mathbf{M}_p^e \mathbf{T}_p^{p+1} \mathbf{B}^{p+1} + (\mathbf{C}^e)^T \mathbf{M}_{p+1}^e \mathbf{B}^{p+1}\\ &= ((\mathbf{P}^e)^T \mathbf{M}_p^e \mathbf{T}_p^{p+1} + (\mathbf{C}^e)^T \mathbf{M}_{p+1}^e)\mathbf{B}^{p+1} = (\mathbf{R}^e)^T \overline{\mathbf{M}}_{p+1}^e \mathbf{B}^{p+1},\end{aligned} \tag{22}$$

where

$$\mathbf{R}^e = \begin{bmatrix} \mathbf{P}^e \\ \mathbf{C}^e \end{bmatrix}, \ \overline{\mathbf{M}}_e = \begin{bmatrix} \mathbf{M}_p^e \mathbf{T}_p^{p+1} \\ \mathbf{M}_{p+1}^e \end{bmatrix}. \tag{23}$$

$\mathbf{R}^e$ are the control points, $\overline{\mathbf{M}}_{p+1}^e$ is the Bézier extraction matrix, and $\mathbf{T}_p^{p+1}$ is obtained from Eqn. (20). Analogously we can get the same expression for Eqn. (18) when p is even, except that

$$\mathbf{R}^e = \begin{bmatrix} \mathbf{C}^e \\ \mathbf{P}^e \end{bmatrix}. \tag{24}$$

As in Section 3.1, partition of unity is not satisfied necessarily. We use weighted T-splines in order to restore partition of unity, namely, $\overline{\mathbf{M}}_{p+1}^e$ is changed to $\widehat{\mathbf{M}}_{p+1}^e$ by normalizing each column of $\widehat{\mathbf{M}}_{p+1}^e$ with Eqn. (6). Thus the hybrid-degree weighted T-spline is defined as

$$\mathbf{x}^e = (\mathbf{R}^e)^T \widehat{\mathbf{M}}_{p+1}^e \mathbf{B}^{p+1}. \tag{25}$$

The calculated hybrid T-splines with different hybrid boundaries of $p = 3$ and $p = 2$ are given in Fig. 6(j - m).

With the developed way to introduce zero-interval length edges and define basis functions of degree p+1, the calculated T-spline surface is C^p-continuous at the p-refined region except the hybrid boundaries. It is C^{p-1}-continuous at the unchanged region, the transition region, and the hybrid boundaries.

Remark 3.2. For now, the degree difference of basis functions over the transition region is one. It is also possible to make the hybrid-degree weighted T-splines more general by introducing further p-refined basis functions to support the transition region, such as basis functions of degree $p + 2$, or even higher. For the transition regions, the surface continuity is determined by the basis function with the lowest degree. The degree of extracted Bézier element is determined by the basis function with the highest degree.

Handling Extraordinary Nodes. Hybrid-degree weighted T-splines can also be used to perform local p-refinement to arbitrary topology surfaces with extraordinary nodes. Till now, the developed algorithms to deal with extraordinary nodes always use cubic basis functions [39, 41, 60]. Since extraordinary nodes influence their two-ring neighborhoods, we can apply interior boundaries to enclose the two-ring neighborhood of each extraordinary node. Then beyond the hybrid boundaries, we define T-splines of $p = 2$ or $p = 4$. In this way, we can define hybrid T-spline surfaces of odd and even degrees on arbitrary shape topology. However, directly using even degree basis functions to deal with extraordinary nodes is still an open problem.

Remark 3.3. The main limitation of hybrid-degree weighted T-splines is that the geometry may be slightly changed after the local p-refinement. The reason is that we are defining basis functions of higher degree without sacrificing the surface continuity, and basis functions of different degree have support over the transition region. Zero-length interval edges are only introduced to the hybrid boundaries, not to all the faces in the p-refined region.

If we introduce the zero-length interval edges to all the p-refined region, the surface change will only exist in the transition region. However this limitation will not bring trouble to analysis of 2D flat surfaces or 3D solids if the local p-refinement is performed such that the geometry boundary is not modified.

4. Results and Discussion

Here we first test hybrid-degree weighted T-splines with a common patch test of linear elasticity. Then, we use odd-, even- and hybrid-degree weighted T-splines to solve a classical benchmark problem that can be physically interpreted as a steady heat conduction. Finally, four other hybrid-degree weighted T-spline surfaces are given.

4.1. Isogeometric Analysis using Hybrid-Degree Weighted T-splines

We perform a patch test on a unit square. The Young's modulus is $E = 1.0$, and the Poisson's ratio is $\nu = 0.3$. Regarding the boundary conditions, the displacement in x direction is set to be 0 and 0.1 on the left and right boundaries, respectively. The displacement in y direction is set to be 0 on the bottom boundary and homogeneous Neumann boundary conditions are imposed elsewhere. Hybrid-degree weighted T-splines with interior and extended hybrid boundaries as shown in Fig. 6(a, c) are tested here. The results are shown in Fig. 8. We obtain linearly distributed displacement along x and y directions and uniform stress in x direction. The analysis results give the exact solution to the problem up to the machine precision.

The second problem solved here is a heat transfer problem defined over an L-shaped domain governed by the Laplace equation $\Delta u = 0$ with ho-

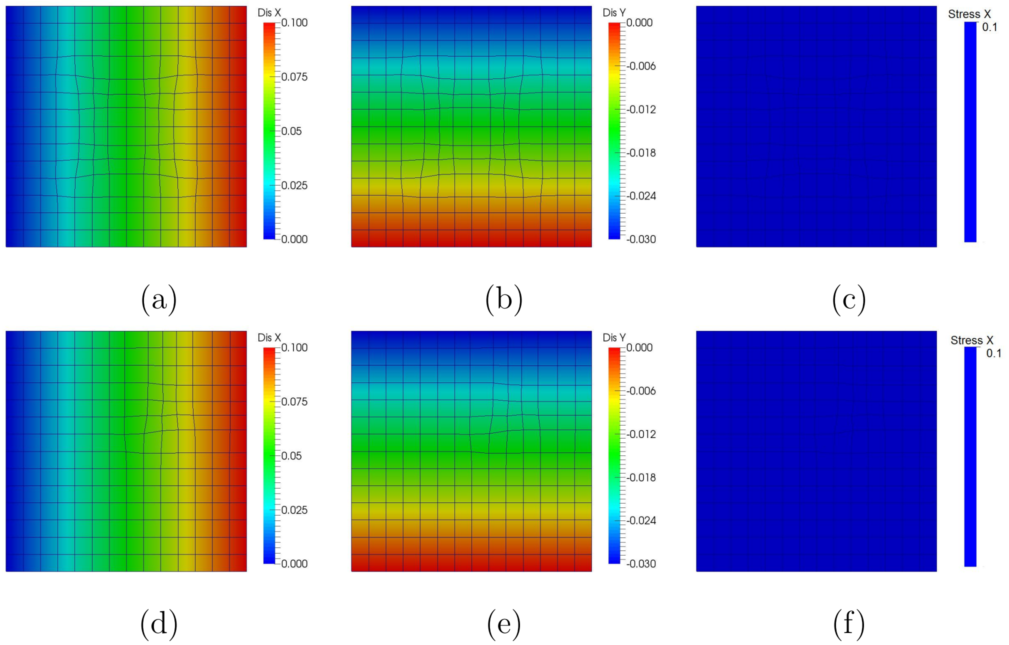

(a) (b) (c)

(d) (e) (f)

Figure 8: Patch test with weighted hybrid-degree T-spline with interior hybrid boundary (a-c) and extend hybrid boundary (d-f). (a, d) Displacement along x direction; (b, e) displacement in y direction; and (c, f) stress int x direction.

mogeneous Dirichlet boundary conditions on the re-entrant edges. Proper Neumann boundary conditions are imposed on the remaining boundaries so that the exact solution in polar coordinates (r, θ) is

$$u(r, \theta) = r^{2/3} \sin(2\theta/3), \ \ r > 0 \text{ and } 0 \leq \theta \leq 3\pi/2. \tag{26}$$

The problem setting is shown in Fig. 9(a). The domain is parameterized with locally h-refined T-splines of $p = 3$ and $p = 4$ first. Then the hybrid-degree weighted T-splines are obtained by performing local p-refinement to the T-spline with $p = 3$ near the re-entrant corner. Fig. 9(b) shows the refined meshes with hybrid degrees $p = 3, 4$, respectively.

Fig. 9(c) shows the solution over the domain. Fig 9(d) shows the relative

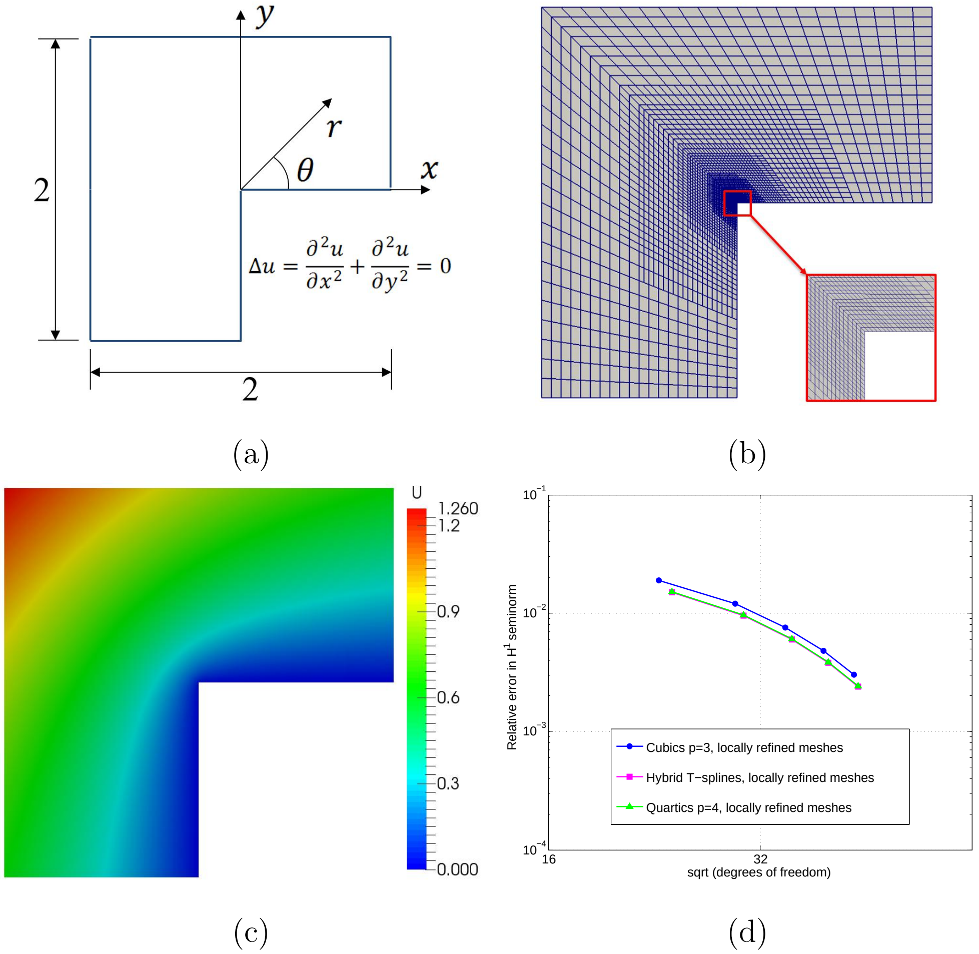

Figure 9: Isogeometric analysis of the Laplace equation over an L-shaped domain with re-entrant corner. (a) Geometry and problem settings; (b) Bézier elements with 4 levels of local h-refinement and local p-refinement with hybrid degrees $p = 3, 4$ near the re-entrant corner; (c) solution field over the domain; (d) convergence curves of the three meshes.

error of H^1 semi-norm with respect to the square root of degrees of freedom. With local p-refinement, hybrid-degree weighted T-splines perform better than T-splines of $p = 3$. Hybrid-degree weighted T-splines generate results as good as T-splines of $p = 4$. The reason is that the maximal error happens at the re-entrant corner where the first partial derivatives of the solution field have a singularity. Therefore, we extract Bézier elements of $p = 4$ from hybrid-degree weighted T-splines for the region close to the re-entrant corner in order to improve the performance. In conclusion, local p-refinement gives additional flexibility to T-splines in order to enhance its efficiency in analysis.

Remark 4.1. Note that both h- and p-refinement are performed close to the singularity in the second problem. This is done in order to decrease the relative error of the H^1 seminorm which is concentrated near the singularity. However, in more complex settings, such as compressible gas dynamics, other hp-refinement strategies are known to perform better [61]. It is quite widespread to use local h-refinement where the solution is rough and to use local p-refinement in the rest of the domain where the solution is smooth.

4.2. Open and Closed Hybrid-Degree Weighted T-spline Surfaces

Here we show four hybrid-degree weighted T-spline surfaces, including two open surfaces as shown in Fig. 10 and two high genus closed T-spline surfaces as shown in Fig. 11.

A square model is shown in Fig. 10(a), with a combination of degrees 2, 3, 4 and 5 basis functions, marked with different colors. Extended hybrid boundaries exist in this model. Hybrid-degree weighted T-splines can combine basis functions of different degrees using different layers of transition regions. In Fig. 10(b), a circle model is provided with a combination of degrees 3, 4 and 5 basis functions. Interior hybrid boundaries exist in this model. There are 4 valance-3 extraordinary nodes. T-splines of $p = 3$ are used to handle the extraordinary nodes. After local p-refinement with hybrid-degree weighted T-splines, the surface is changed along the radial direction

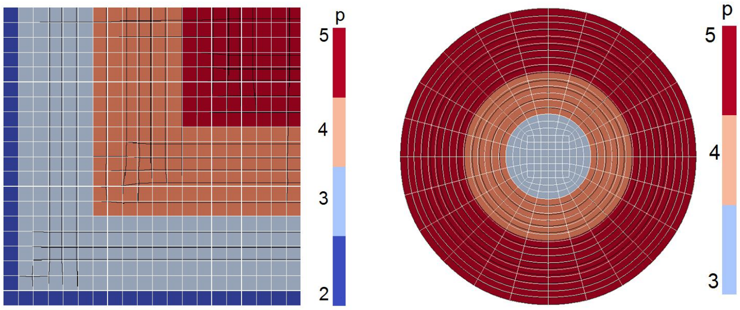

(a) (b)

Figure 10: Open surface hybrid-degree weighted T-spline models. (a) A square model with extended hybrid boundaries and the difference before (white lines) and after refinement (black lines); and (b) a circle model with interior hybrid boundaries and the difference before (white lines) and after refinement (black lines).

near the hybrid boundaries. In Fig. 10, the white and black lines show the difference before and after local p-refinement. For open surface models, with the scheme to calculate the control points, the local region around the hybrid boundaries in the interior of the geometry is changed. The boundary of the geometry remains unchanged after refinement.

Two closed surface models with extraordinary nodes are given in Fig. 11. The Tetra model in Fig. 11(a) has eight valance-6 extraordinary nodes. The original T-spline surface is of degree 3. After local p-refinement, the hybrid-degree weighted T-spline is shown in Fig. 11(b), with the comparison before and after refinement. Fig. 11(d-f) shows the Genus-three model before and after local p-refinement. In this model, we set the two-ring neighborhood of the four valance-8 extraordinary nodes as degree 3. For all the other regions, the surface is of degree 4. With hybrid-degree weighted T-splines, we can generate T-spline surfaces with basis functions of different degrees in one

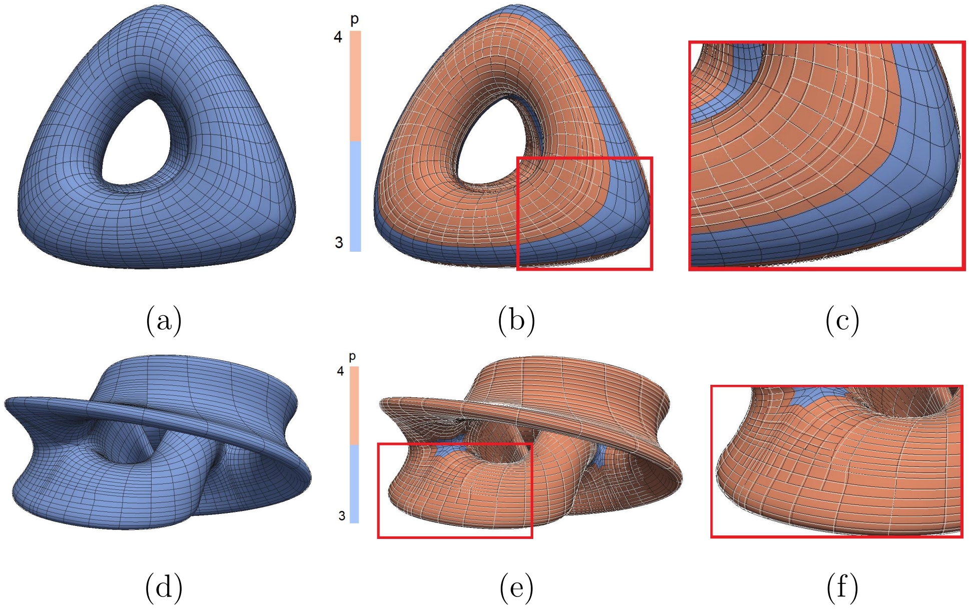

(a) (b) (c)

(d) (e) (f)

Figure 11: Tetra model (a-c) and Genus-three model (d-f) of hybrid-degree weighted T-splines. (a, d) Original model of degree 3; (b, e) local p-refinement results, where the white and black lines show the difference of Bézier elements before and after refinement; and (c, f) show the zoom-in of (b, e).

model.

5. Conclusions and Future Work

In conclusion, in this paper we develop a new algorithm to generate hybrid-degree weighted T-splines which can be used in isogeometric analysis. Weighted T-splines of arbitrary degree are proposed which satisfy all the analysis-suitable requirements. Hybrid-degree weighted T-splines are developed with two types of hybrid boundaries for local p-refinement. Both odd- and even-degree T-spline basis functions are defined. The p-refined regions and unchanged regions are connected via transition regions. Both

p-refined basis functions and original basis functions have support over the transition regions, over which the hybrid-degree weighted T-splines are defined. The transition region has basis functions of the same degree as the p-refined region, and the same surface continuity as the unchanged region. Bézier elements of different degrees are extracted for isogeometric analysis. The Laplace equation is solved on an L-shaped domain, which is parameterized with odd-, even-, and hybrid-degree T-splines. Hybrid T-splines provide better performance after local p-refinement. In the future, we are planning to develop a better control point calculation algorithm to decrease the surface change after local p-refinement.

Acknowledgements

Lei Liu and Yongjie Jessica Zhang were supported in part by the PECASE Award N00014-14-1–0234. Hugo Casquero and Hector Gomez were partially supported by the European Research Council through the FP7 Ideas Starting Grant (project # 307201). Hector Gomez was also partially supported by Ministerio de Econoía y Competitividad (project # DPI2013-44406-R), confinanced with FEDER funds.

References

[1] T. J. R. Hughes, J. A. Cottrell, Y. Bazilevs, Isogeometric analysis: CAD, finite elements, NURBS, exact geometry, and mesh refinement, Computer Methods in Applied Mechanics and Engineering 194 (2005) 4135–4195.

[2] L. A. Piegl, W. Tiller, The NURBS Book, 2nd ed., Springer-Verlag, New York, 1997.

[3] J. A. Cottrell, T. J. R. Hughes, Y. Bazilevs, Isogeometric analysis: toward integration of CAD and FEA, Wiley, 2009.

[4] G. Xu, B. Mourrain, R. Duvigneau, A. Galligo, Analysis-suitable volume parameterization of multi-block computational domain in isogeometric applications, Computer-Aided Design 45 (2) (2013) 395–404.

[5] T. W. Sederberg, J. Zheng, A. Bakenov, A. Nasri, T-splines and T-NURCCs, ACM Transactions on Graphics 22 (3) (2003) 477–484.

[6] Y. Bazilevs, V. M. Calo, J. A. Cottrell, J. A. Evans, T. J. R. Hughes, S. Lipton, M. A. Scott, T. W. Sederberg, Isogeometric analysis using T-splines, Computer Methods in Applied Mechanics and Engineering 199 (5-8) (2010) 229–263.

[7] H. Casquero, L. Liu, Y. Zhang, A. Reali, H. Gomez, Isogeometric collocation using analysis-suitable T-splines of arbitrary degree, submitted, 2015.

[8] S. Lipton, J. A. Evans, Y. Bazilevs, T. Elguedj, T. J. R. Hughes, Robustness of isogeometric structural discretizations under severe mesh distortion, Computer Methods in Applied Mechanics and Engineering 199 (58) (2010) 357–373.

[9] I. Akkerman, Y. Bazilevs, V. M. Calo, T. J. R. Hughes, S. Hulshoff, The role of continuity in residual-based variational multiscale modeling of turbulence, Computational Mechanics 41 (2008) 371–378.

[10] Y. Bazilevs, V. M. Calo, T. J. R. Hughes, Y. Zhang, Isogeometric fluid-structure interaction: theory, algorithms, and computations, Computational Mechanics 43 (1) (2008) 3–37.

[11] Y. Zhang, Y. Bazilevs, S. Goswami, C. L. Bajaj, T. J. R. Hughes, Patient-specific vascular NURBS modeling for isogeometric analysis of blood flow, Computer Methods in Applied Mechanics and Engineering 196 (29-30) (2007) 2943–2959.

[12] Y. Bazilevs, V. M. Calo, Y. Zhang, T. J. R. Hughes, Isogeometric fluid-structure interaction analysis with applications to arterial blood flow, Computational Mechanics 38 (4-5) (2006) 310–322.

[13] Y. Bazilevs, M.-C. Hsu, I. Akkerman, S. Wright, K. Takizawa, B. Henicke, T. Spielman, T. Tezduyar, 3D simulation of wind turbine rotors at full scale. part I: Geometry modeling and aerodynamics, International Journal for Numerical Methods in Fluids 65 (2011) 207–235.

[14] Y. Bazilevs, M.-C. Hsu, J. Kiendl, R. Wuchner, K.-U. Bletzinger, 3D simulation of wind turbine rotors at full scale. part II: Fluid-structure interaction modeling with composite blades, International Journal for Numerical Methods in Fluids 65 (2011) 236–253.

[15] J. Bueno, C. Bona-Casas, Y. Bazilevs, H. Gomez, Interaction of complex fluids and solids: theory, algorithms and application to phase-change-driven implosion, Computational Mechanics 55 (6) (2015) 1105–1118.

[16] D. Kamensky, M.-C. Hsu, D. Schillinger, J. A. Evans, A. Aggarwal, Y. Bazilevs, M. S. Sacks, T. J. R. Hughes, An immersogeometric vari-

ational framework for fluid-structure interaction: application to bioprosthetic heart valves, Computer Methods in Applied Mechanics and Engineering 284 (2015) 1005–1053.

[17] M.-C. Hsu, D. Kamensky, Y. Bazilevs, M. S. Sacks, T. J. R. Hughes, Fluid-structure interaction analysis of bioprosthetic heart valves: significance of arterial wall deformation, Computational Mechanics 54 (2014) 1055–1071.

[18] M.-C. Hsu, D. Kamensky, F. Xu, J. Kiendl, C. Wang, M. Wu, J. Mineroff, A. Reali, Y. Bazilevs, M. S. Sacks, Dynamic and fluid-structure interaction simulations of bioprosthetic heart valves using parametric design with T-splines and Fung-type material models, Computational Mechanics 55 (2015) 1211–1225.

[19] H. Casquero, C. Bona-Casas, H. Gomez, A NURBS-based immersed methodology for fluid-structure interaction, Computer Methods in Applied Mechanics and Engineering 284 (0) (2015) 943–970.

[20] H. Casquero, L. Liu, C. Bona-Casas, Y. Zhang, H. Gomez, A hybrid variational-collocation immersed method for fluid-structure interaction using unstructured T-splines, International Journal for Numerical Methods in Engineering (2015) doi:10.1002/nme.5004.

[21] H. Gomez, V. M. Calo, Y. Bazilevs, T. J. R. Hughes, Isogeometric analysis of the Cahn-Hilliard phase-field model, Computer Methods in Applied Mechanics and Engineering 197 (49-50) (2008) 4333–4352.

[22] H. Gomez, T. J. R. Hughes, X. Nogueira, V. M. Calo, Isogeometric analysis of the isothermal Navier-Stokes-Korteweg equations, Computer Methods in Applied Mechanics and Engineering 199 (2010) 1828–1840.

[23] J. Kiendl, K.-U. Bletzinger, J. Linhard, R. Wuchner, Isogeometric shell analysis with Kirchhoff-Love elements, Computer Methods in Applied Mechanics and Engineering 198 (2009) 3902–3914.

[24] J. Kiendl, M.-C. Hsu, M. C. H. Wu, A. Reali, Isogeometric Kirchhoff-Love shell formulations for general hyperelastic materials, Computer Methods in Applied Mechanics and Engineering 291 (2015) 280–303.

[25] H. Gomez, X. Nogueira, An unconditionally energy-stable method for the phase field crystal equation, Computer Methods in Applied Mechanics and Engineering 249 (2012) 52–61.

[26] G. Vilanova, I. Colominas, H. Gomez, Capillary networks in tumor angiogenesis: From discrete endothelial cells to phase-field averaged descriptions via isogeometric analysis, International Journal for Numerical Methods in Biomedical Engineering 29 (2013) 1015–1037.

[27] G. Vilanova, I. Colominas, H. Gomez, Coupling of discrete random walks and continuous modeling for three-dimensional tumor-induced angiogenesis, Computational Mechanics 53 (2013) 449–464.

[28] F. Auricchio, L. B. Da Veiga, T. J. R. Hughes, A. Reali, G. Sanglli, Isogeometric collocation methods, Mathematical Models and Methods in Applied Sciences 20 (11) (2010) 2075–2107.

[29] D. Schillinger, J. A. Evans, A. Reali, M. A. Scott, T. J. R. Hughes, Isogeometric collocation: cost comparison with Galerkin methods and extension to adaptive hierarchical NURBS discretizations, Computer Methods in Applied Mechanics and Engineering 267 (0) (2013) 170–232.

[30] H. Gomez, A. Reali, G. Sangalli, Accurate, efficient, and (iso)geometrically flexible collocation methods for phase-field models, Journal of Computational Physics 262 (2014) 153–171.

[31] A. Reali, H. Gomez, An isogeometric collocation approach for Bernoulli-Euler beams and Kirchhoff plates, Computer Methods in Applied Mechanics and Engineering 284 (2015) 623–636.

[32] C. Anitescu, Y. Jia, Y. Zhang, T. Rabczuk, An isogeometric collocation method using superconvergent points, Computer Methods in Applied Mechanics and Engineering 284 (2015) 1073–1097.

[33] X. Li, M. A. Scott, Analysis-suitable T-splines: characterization, refineability, and approximation, Mathematical Models and Methods in Applied Sciences 24 (06) (2014) 1141–1164.

[34] X. Li, Some properties for analysis-suitable T-splines, Journal of Computational Mathematics 33 (4) (2015) 428–442.

[35] A. Buffa, D. Cho, G. Sangalli, Linear independence of the T-spline blending functions associated with some particular T-meshes, Computer Methods in Applied Mechanics and Engineering 199 (23-24) (2010) 1437–1445.

[36] X. Li, J. Zheng, T. W. Sederberg, T. J. R. Hughes, M. A. Scott, On linear independence of T-spline blending functions, Computer Aided Geometric Design 29 (1) (2012) 63–76.

[37] L. Beirão da Veiga, A. Buffa, G. Sangalli, R. Vázquez, Analysis-suitable T-splines of arbitrary degree: definition, linear independence and approximation properties, Mathematical Models and Methods in Applied Sciences 23 (11) (2013) 1979–2003.

[38] A. Bressan, A. Buffa, G. Sangalli, Characterization of analysis-suitable T-splines, Computer Aided Geometric Design (2015) doi:10.1016/j.cagd.2015.06.007.

[39] M. A. Scott, R. N. Simpson, J. A. Evans, S. Lipton, S. P. A. Bordas, T. J. R. Hughes, T. W. Sederberg, Isogeometric boundary element analysis using unstructured T-splines, Computer Methods in Applied Mechanics and Engineering 254 (0) (2013) 197–221.

[40] L. Liu, Y. Zhang, X. Wei, Weighted T-splines with application in reparameterizing trimmed NURBS surfaces, Computer Methods in Applied Mechanics and Engineering 295 (2015) 108–126.

[41] L. Liu, Y. Zhang, X. Wei, Handling extraordinary nodes with weighted T-spline basis functions, in: 24th International Meshing Roundtable, accepted, 2015.

[42] T. W. Sederberg, D. L. Cardon, G. T. Finnigan, N. S. North, J. Zheng, T. Lyche, T-spline simplification and local refinement, in: ACM SIGGRAPH, 2004, pp. 276–283.

[43] M. A. Scott, X. Li, T. W. Sederberg, T. J. R. Hughes, Local refinement of analysis-suitable T-splines, Computer Methods in Applied Mechanics and Engineering 213-216 (0) (2012) 206–222.

[44] P. Morgenstern, D. Peterseim, Analysis-suitable adaptive T-mesh refinement with linear complexity, Computer Aided Geometric Design 34 (0) (2015) 50–66.

[45] P. Morgenstern, 3D Analysis-suitable T-splines: definition, linear independence and m-graded local refinement (2015), ArXiv e-printsarXiv:1505.05392, 2015.

[46] E. J. Evans, M. A. Scott, X. Li, D. C. Thomas, Hierarchical T-splines: Analysis-suitability, Bézier extraction, and application as an adaptive basis for isogeometric analysis, Computer Methods in Applied Mechanics and Engineering 284 (2015) 1–20.

[47] C. Giannelli, B. Jüttler, H. Speleers, THB-splines: the truncated basis for hierarchical splines, Computer Aided Geometric Design 29 (2012) 485–498.

[48] X. Wei, Y. Zhang, T. J. R. Hughes, M. A. Scott, Truncated hierarchical Catmull-Clark surface with local refinement, Computer Methods in Applied Mechanics and Engineering 291 (2015) 1–20.

[49] X. Wei, Y. Zhang, T. J. R. Hughes, M. A. Scott, Extended truncated hierarchical Catmull-Clark subdivision, Computer Methods in Applied Mechanics and Engineering, accepted, 2015.

[50] H. Prautzsch, Degree elevation of B-spline curves, Computer Aided Geometric Design 1 (2) (1984) 193–198.

[51] E. Cohen, T. Lyche, L. L. Schumaker, Algorithms for degree-raising of splines, ACM Transactions on Graphics 4 (3) (1985) 171–181.

[52] E. Cohen, T. Lyche, L. L. Schumaker, Degree raising for splines, Journal of Approximation Theory 46 (2) (1986) 170–181.

[53] H. Prautzsch, B. Piper, A fast algorithm to raise the degree of spline curves, Computer Aided Geometric Design 8 (4) (1991) 253–265.

[54] L. Piegl, W. Tiller, Software-engineering approach to degree elevation of B-spline curves, Computer-Aided Design 26 (1) (1994) 17–28.

[55] T. W. Sederberg, J. Zheng, X. Song, Knot intervals and multi-degree splines, Computer Aided Geometric Design 20 (7) (2003) 455–468.

[56] W. Shen, G. Wang, A basis of multi-degree splines, Computer Aided Geometric Design 27 (1) (2010) 23–35.

[57] X. Li, Z. Huang, Z. Liu, A geometric approach for multi-degree spline, Journal of Computer Science and Technology 27 (4) (2012) 841–850.

[58] M. A. Scott, M. J. Borden, C. V. Verhoosel, T. W. Sederberg, T. J. R. Hughes, Isogeometric finite element data structures based on Bézier extraction of T-splines, International Journal for Numerical Methods in Engineering 88 (2) (2011) 126–156.

[59] R. Goldman, T. Lyche, Knot insertion and deletion algorithms for B-spline curves and surfaces, Society for Industrial and Applied Mathematics–Philadelphia, 1993.

[60] W. Wang, Y. Zhang, G. Xu, T. J. R. Hughes, Converting an unstructured quadrilateral/hexahedral mesh to a rational T-spline, Computational Mechanics 50 (1) (2012) 65–84.

[61] S. Giani, P. Houston, Anisotropic *hp*-adaptive discontinuous galerkin finite element methods for compressible fluid flows, International Journal of Numerical Analysis and Modeling 9 (4) (2012) 928–949.